Development of reduced activation austenitic stainless steel containing high density of nanosized precipitates for fusion energy application

Hyun Joon Eom, Ji Ho Shin, Byeong Seo Kong, Chae Won Jeong, Changheui Jang*
Dept. of Nuclear and Quantum Engineering, KAIST, Daejeon, Rep. of Korea
**Corresponding Author: chjang@kaist.ac.kr*

1. Introduction

Development of low activation materials is important in the nuclear fusion reactors in that long-lived isotopes should be reduced to enable the shallow land burial after the operation [1]. In that sense, ferritic-martensitic steels (FMSs) or oxide-dispersion strengthened FMSs (FM-ODSs) have been considered as candidate structural materials for the fusion reactors [2]. On the other hand, austenitic stainless steels (SSs) are also attractive structural materials for the fusion reactors because of their superior corrosion resistance, creep strength, and mechanical properties at high temperature compared to the FMSs or FM-ODSs [3]. However, under the neutron irradiation, these austenitic SSs are considered to suffer from various radiation-induced damages such as dislocation loops, precipitation and the formation of voids [4]. In particular, with the formation of voids, austenitic SSs become susceptible to the void swelling, which causes it hard to be used in high temperature and high neutron irradiation environments such as blankets in fusion reactors.

Meanwhile, many strengthening methods are suggested from various reports to enhance the radiation resistance of the alloys. Among them, introducing precipitates which can act as sink sites for radiation-induced defects is one of the widely used methods to develop low activation alloy with excellent radiation resistance [5, 6]. Recently, considering this effect of precipitates on the radiation resistance of the alloy, authors have developed an alloy (ARES-F3) with uniformly distributed nanosized tantalum carbide (TaC) in austenitic matrix. In this study, to investigate the effect of precipitates on the void swelling resistance of the alloy, commercial 316 SS and newly developed ARES-F3 alloy were irradiated with heavy ions, and the void swelling results were compared to each other.

2. Alloy design and Experimental results

2.1 Alloy design

The design of this model alloy aimed to improve the radiation resistance by forming TaC precipitates in austenite matrix. The Cr content was selected to be near 15 wt.% for the corrosion resistance. In addition, Ni and Mn contents were selected to make the fully austenitic structure balancing with the Cr content. As the Ni content increased, the low radiation property of this developed alloy deteriorated. Therefore, the Ni content was minimized to be near 7 wt.% and the stability of the austenite matrix was adjusted by increasing the Mn content to be near 11 wt.%. Meanwhile, the addition of Ta and C was to form nanosized TaC precipitates with uniform distribution. Among various precipitate forming elements, TaC exhibited the greatest resistance under the thermal aging, creep, and ion irradiation condition [7]. So, the Ta content was selected to be near 0.4 – 0.5 wt.%, while the C content was selected to be near 0.04 wt.% to form enough amount of TaC precipitates for enhancing the radiation resistance after the precipitation heat treatment based on the commercial Thermo-Calc software (TCFE-9 database). The Si content was minimized to prevent the coarsening of precipitates, and other elements such as P and S were considered as impurities which should be also minimized. Considering this whole design concept, the final target chemical compositional range of the developed alloy was Fe – 15Cr – 7Ni – 11Mn – 0.45Ta – 0.04C (wt.%).

2.2 Experimental results

The ingot of this developed alloy with the target chemical composition was prepared through vacuum induction melting. This rectangular-bar type ingot has a dimension of 130 mm × 130 mm × 320 mm and its accurate chemical composition was analyzed through the inductively coupled plasma atomic emission spectroscopy (ICP-AES) and the results are shown in **Table 1**. Equilibrium phase fraction of this alloy with the real chemical composition along temperature are also shown in **Fig. 1** using the Thermo-Calc software. This alloy was conducted with 4 passes of hot rolling above the non-recrystallization temperature (T_{NR}) and 2 passes below T_{NR}. Additional precipitation heat treatment was then conducted to form uniformly distributed fine TaC precipitates in the vicinity of dislocation tangles from the previous hot rolling process. This controllable thermo-mechanical processing was proposed by the previous publication [8].

Table 1
Chemical composition of the ARES-F3 alloy in weight percent (wt.%). [a]

Fe	Cr	Ni	Mn	Ta	C	Si	P	S
Bal.	15.13	7.17	11.16	0.48	0.039	0.22	0.001	0.002

[a] ICP-AES, C/S – KS D 1804/1803

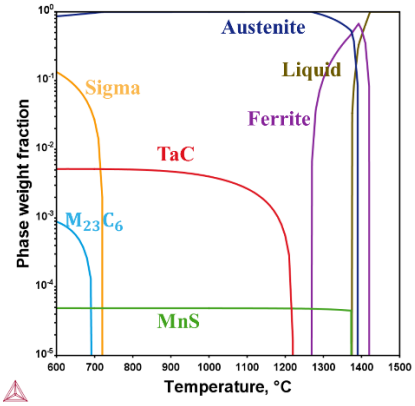

Fig. 1 Calculation of phase fraction result based on ICP-AES analysis on the ingot along the temperature using Thermo-Calc (TCFE-9 database).

For observing the initial microstructure of the ARES-F3 alloy, thin foil specimens with a diameter 3 mm were machined and mechanically polished to a thickness of ~100 μm. Then, the specimens were subjected to twin-jet electropolishing at –30 ℃ with a current of ~0.1 A in a solution of 10% perchloric acid + 90% methanol. High resolution TEM (HRTEM) was performed using a FEI-Talos F200X equipped with a Bruker Quantax energy dispersive X-ray spectroscopy (EDS) at 200 kV. To estimate the thickness of each TEM sample, the electron mean free path was measured by electron energy loss spectroscopy (EELS) [9].

The TEM micrographs of the ARES-F3 alloy are shown in **Fig. 2**. As shown in **Fig. 2**a, the fine precipitates were observed in the vicinity of dislocation tangles which act as the nucleation site during the heat treatment. High-angle annular dark-field (HAADF) image and EDS mapping images show that these precipitates are TaC precipitates, which are semi-coherent with the austenitic matrix. In addition, HRTEM image (**Fig. 2**d) and the corresponding fast Fourier transform (FFT) pattern along [011] zone (**Fig. 2**e) were used for the detailed analysis of characteristics of the TaC precipitates with an average diameter of ~5.7 nm and an average number density of ~1.7×10^{23} m^{-3}.

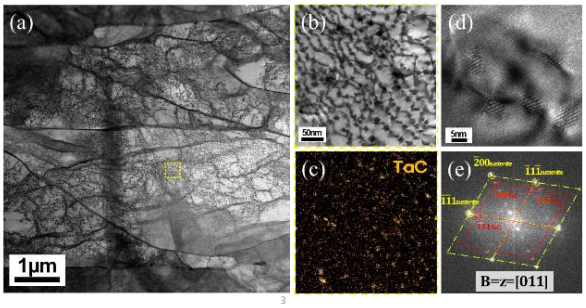

Fig. 2 TEM micrographs of the ARES-F3 alloy: (a) bright-field TEM (BFTEM) image with the corresponding (b) HAADF and (c) EDS mapping image for the yellow dotted area in (a). (d) HRTEM image and corresponding (e) FFT pattern of TaC precipitates along the [001] zone.

Heavy ion irradiation was conducted at 500 ℃ for 316 SS and ARES-F3 alloy with a defocused beam without raster scanning. Based on Stopping and Range of Ions in Matter (SRIM) method using a displacement energy of 40 eV in Kinchin-Pease (K–P) model [10], the depth profiles of the radiation damage were calculated and plotted with the cross-sectional TEM image of those irradiated alloys with voids, as shown in **Fig. 3**. Targeted damage was 200 dpa at the 600 nm depth from the surface considered as plateau region with a dose rate of ~5×10^{-4} dpa/s (calculated at 600 nm depth).

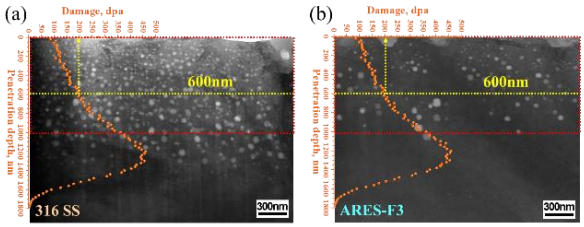

Fig. 3 Cross-sectional BFTEM images showing the voids in irradiated (a) 316 SS and (b) ARES-F3. The irradiation direction is from top to bottom and calculated SRIM result is superimposed for each.

From these cross-sectional TEM images, the number density and size of the voids from the depth of 400 nm to 800 nm were carefully analyzed and void swelling was calculated with the following equation [11]:

$$Void\ swelling\ (\%) = \frac{\frac{\pi}{6}\sum_{i=1}^{N} d_i^3}{A\times t - \frac{\pi}{6}\sum_{i=1}^{N} d_i^3} \times 100, \qquad (1)$$

where A is the area, t is the thickness of the sample, d_i is the diameter of each voids, and N is the total number of voids in given area. The average number density, size of voids and void swelling were measured along the depth and dpa respectively, as shown in **Fig. 4**. According to **Fig. 4**a **and Fig. 4**b, they clearly show that void number density is far higher in the 316 SS, while void size is similar or larger in the ARES-F3. And **Fig. 4**c finally shows that void swelling is much larger for 316 SS due to its high number density, which can be said that TaC precipitates play a key role in enhancing void swelling resistance compared to the irradiated 316 SS.

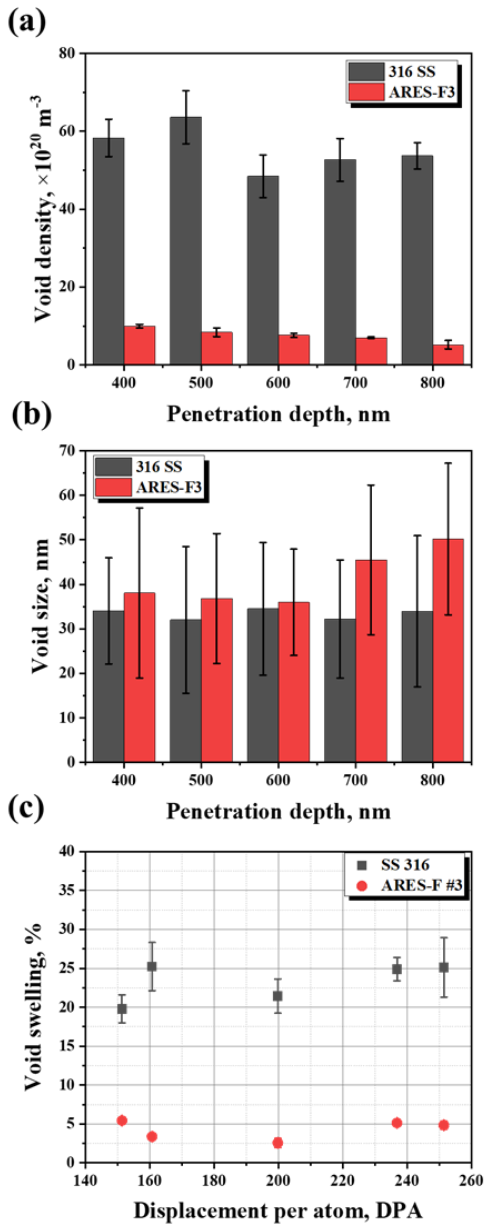

Fig. 4 (a) Average void density, (b) void size, and (c) void swelling of 316 SS and ARES-F3 alloy along the penetration depth or displacement per atom.

3. Summary

Newly developed ARES-F3 alloy and commercial 316 SS are irradiated by the heavy ion to investigate the effect of fine TaC precipitates on void swelling resistance. Analyzing the voids in the irradiated 316 SS and ARES-F3 alloy shows that nanosized TaC precipitates with uniform and dense distribution can work as radiation-induced defect sink to reduce the magnitude of void swelling in austenitic matrix with extreme irradiation environment. Meanwhile, further analyses would be needed to investigate the other properties after the irradiation such as irradiation embrittlement.

REFERENCES

[1] U.o.W.-.-M.F.T. Institute, University of Wisconsin Fusion Technology Institute, University of Wisconsin Fusion Technology Institute.
[2] S.J. Zinkle, L.L. Snead, Designing radiation resistance in materials for fusion energy, Annual Review of Materials Research 44 (2014) 241-267.
[3] K.H. Lo, C.H. Shek, J. Lai, Recent developments in stainless steels, Materials Science and Engineering: R: Reports 65(4-6) (2009) 39-104.
[4] N.K. Kumar, C. Li, K. Leonard, H. Bei, S. Zinkle, Microstructural stability and mechanical behavior of FeNiMnCr high entropy alloy under ion irradiation, Acta Materialia 113 (2016) 230-244.
[5] W. Kesternich, J. Rothaut, Reduction of helium embrittlement in stainless steel by finely dispersed TiC precipitates, Journal of Nuclear Materials 104 (1981) 845-852.
[6] E. Lee, L. Mansur, Fe–15Ni–13Cr austenitic stainless steels for fission and fusion reactor applications. III. Phase stability during heavy ion irradiation, Journal of nuclear materials 278(1) (2000) 20-29.
[7] L. Tan, T.S. Byun, Y. Katoh, L.L. Snead, Stability of MX-type strengthening nanoprecipitates in ferritic steels under thermal aging, stress and ion irradiation, Acta materialia 71 (2014) 11-19.
[8] J.H. Shin, H.-S. Kim, B.S. Kong, G.O. Subramanian, S. Hong, H.J. Lee, C. Jang, Development of thermo-mechanical processing to form high density of uniformly distributed nanosized carbides in austenitic stainless steels, Materials Science and Engineering: A 775 (2020) 138986.
[9] T. Malis, S. Cheng, R. Egerton, EELS log-ratio technique for specimen-thickness measurement in the TEM, Journal of electron microscopy technique 8(2) (1988) 193-200.
[10] U. Saha, K. Devan, S. Ganesan, A study to compute integrated dpa for neutron and ion irradiation environments using SRIM-2013, Journal of Nuclear Materials 503 (2018) 30-41.
[11] Z. Fan, T.-n. Yang, B. Kombaiah, X. Wang, P.D. Edmondson, Y.N. Osetsky, K. Jin, C. Lu, H. Bei, L. Wang, From suppressed void growth to significant void swelling in NiCoFeCr complex concentrated solid-solution alloy, Materialia 9 (2020) 100603.